Solar Energy 197 (2020) 538–545

Contents lists available at ScienceDirect

Solar Energy

journal homepage: www.elsevier.com/locate/solener

High-efficiency solar thermophotovoltaic system using a nanostructure-based selective emitter

Rajendra Bhatt[a,c], Ivan Kravchenko[b], Mool Gupta[a,*]

[a] University of Virginia, Charlottesville, VA 22901, USA
[b] Oak Ridge National Laboratory, Oak Ridge, TN 37831, USA
[c] Science Systems and Applications, Inc., VA 23666, USA

ARTICLE INFO

Keywords:
STPV
Blackbody
TPV cells
Nanostructure
Spectral control

ABSTRACT

In this work, we present the design, fabrication, optimization, and experimental results of a high-efficiency planar solar thermophotovoltaic (STPV) system utilizing a micro-textured absorber and a nanostructure multi-layer metal-dielectric coated selective emitter fabricated on a tungsten (W) substrate. Light absorptance of more than 90% was achieved at visible and near-infrared wavelengths using the microtextured absorbing surface. The nanostructure selective emitter consists of two thin-film optical coatings of silicon nitride (Si_3N_4) and a layer of W in between to increase the surface emissivity in spectral regimes matching the quantum efficiency of the thermophotovoltaic (TPV) cells. Gallium antimonide (GaSb)-based TPV cells are used in our STPV design. The experiment was conducted at different operating temperatures using a high-power continuous wave laser diode stack as a simulated source of concentrated incident radiation. Our experimental setup measured a maximum electrical output power density of 1.71 W/cm^2 at 1676 K STPV temperature, and the overall power conversion efficiency of 8.4% after normalizing the output power density to the emitter area. This is the highest STPV system efficiency reported so far for any experimental STPV device. The incident optical laser power on the absorber side was 131 W. This is equivalent to a solar concentration factor of ~2100, which is within the practical limit and readily achievable with Fresnel lens setup.

1. Introduction

Recently, there has been a renewed interest in the development of solar thermophotovoltaic (STPV) devices (Bierman et al., 2016; Kohiyama et al., 2016; Lenert et al., 2014a; Ungaro et al., 2015), given their potential for high-efficiency solar energy harvesting by utilizing the full solar spectrum. A single-junction solar cell is subject to the Shockley-Queisser (SQ) limit (Shockley and Queisser, 1961), which imposes a fundamental upper bound on its solar-to-electric energy conversion efficiency. According to this limit, the theoretical maximum efficiency for a single-junction cell under standard illumination (air mass of 1.5 and in the absence of concentration) is ~33% for an optimal bandgap of ~1.4 eV (Rühle, 2016). A major contribution to the SQ limit arises from inevitable losses (thermalization and transmission losses) caused by the spectral mismatch between solar radiation and the cell's response. STPV systems aim to achieve efficiencies higher than the SQ limit through the use of an intermediate element that absorbs the broadband sunlight and re-emits the absorbed energy as a narrow-band thermal radiation tuned to directly above the bandgap of the solar cell. Spectrally selective absorbers and emitters can greatly enhance the STPV system efficiency by maximizing the absorption and suppressing the emission of sub-bandgap and excessive energy photons (Rephaeli and Fan, 2009).

Fig. 1a shows a layout of a typical planar STPV system. Unlike conventional solar photovoltaics (PV), STPV utilizes concentrated solar radiation, which is absorbed and reemitted as thermal radiation towards a thermophotovoltaic (TPV) cell through a thermally coupled absorber and emitter pair (Rephaeli and Fan, 2009). Most of the efficiency gain of STPV arises from the spectral control in the emitter. A selective spectral filter placed in between the emitter and the TPV cell reflects the sub-band-gap photons back to the emitter for recycling. An infrared (IR) reflector or heat shield can also be installed on the absorber side to minimize the thermal radiation loss from the absorbing surface (Kohiyama et al., 2016). Effective recycling of the unused thermal radiation greatly enhances the system efficiency. Another key aspect of designing a STPV system is choosing the bandgap of the TPV cells. An optimal bandgap is determined by the thermal emission spectrum, which in turn is controlled by the emitter temperature and

* Corresponding author.
E-mail address: mgupta@virginia.edu (M. Gupta).

https://doi.org/10.1016/j.solener.2020.01.029
Received 21 October 2019; Received in revised form 4 December 2019; Accepted 11 January 2020

Nomenclature

List of symbols and abbreviations

B(λ, T)	Planck's blackbody function
ε_{Eff}	effective emissivity
$\varepsilon_{in\text{-}band}$	in-band emissivity
η_e	thermal extraction efficiency
η_{PV}	photovoltaic conversion efficiency
η_{sel}	spectral selectivity
η_{STPV}	STPV system efficiency
λ	wavelength
λ_{BG}	bandgap wavelength
T	absolute temperature
EQE	external quantum efficiency
eV	electron Volt
FF	fill factor
GaSb	Gallium Antimonide
Ge	germanium
HfO_2	hafnium oxide
InAs	Indium Arsende
InGaAsSb	Indium Gallium Arsenide Antimonide
IR	Infrared
Mo	molybdenum
P_{cond}	power loss due to conduction
P_{conv}	power loss due to convection
P_{in}	incident power
PECVD	plasma-enhanced chemical vapor deposition
P_{ref}	reflected power
P_{rad}	thermally radiated power
PV	photovoltaic
QTH	quartz tungsten halogen
Si	silicon
Si_3N_4	silicon Nitride
SQ	Shockley-Queisser
STPV	solar thermophotovoltaic
Ta	tantalum
TMM	transfer matrix method
TPV	thermophotovoltaic
VF	view factor
W	tungsten

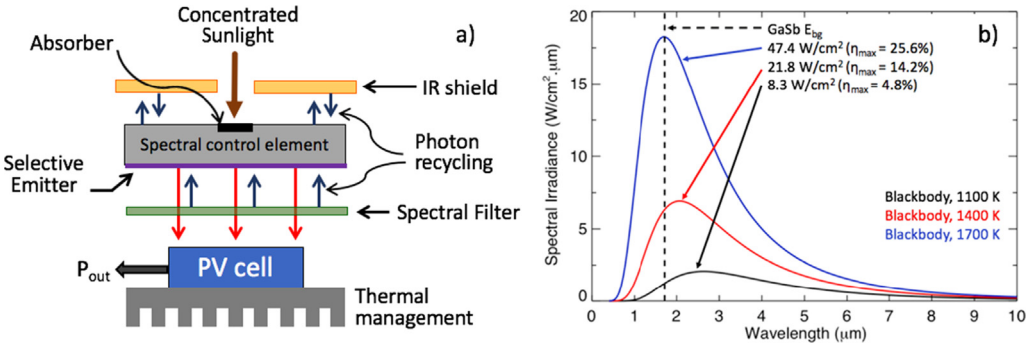

Fig. 1. (a) Layout of a typical planar STPV system. (b) Impact of the spectral distribution of the blackbody power on the conversion efficiency of a GaSb TPV cell.

the spectral characteristics of the emitter surface (Datas, 2015). Low bandgap cells (< 1eV) are preferred because they require lower operating temperatures (< 1800 K) for the emitter. Germanium (Ge), gallium antimonide (GaSb), and indium gallium arsenide antimonide (InGaAsSb) cells are of considerable interest for STPV applications. Fig. 1b illustrates the impact of the STPV temperature on the conversion efficiency of GaSb TPV cells. The blackbody power density at temperatures 1100 K, 1400 K, and 1700 K are shown along with the bandgap wavelength (λ_{BG}) of GaSb. With increasing temperature, the overall radiated power per unit area increases and the peak of the blackbody curve shifts towards shorter wavelengths. Because only photons having wavelengths less than λ_{BG} can be converted to electric energy, the maximum thermal-to-electrical conversion efficiency is limited by the fraction of the total radiated power that is below λ_{BG}. For a blackbody source at 1700 K, the maximum theoretical efficiency of a GaSb TPV cell is only 25.6%. Clearly, a blackbody emitter is not an ideal choice for STPV systems as it radiates a significant fraction of energy above λ_{BG}, thereby highlighting the critical need for a spectrally selective emitter and photon recycling in STPV for boosting the system efficiency. The high incident power density results in thermal stress on the TPV cells. Therefore, a thermal management system, usually water-cooling, is implemented in STPV to keep the TPV cells at room temperature (300 K). STPV systems are scalable, reliable (no moving parts), and versatile in utilizing alternative sources of heat, such as radio-isotope heaters, thermal storage systems, combustible materials, etc., as inputs.

The ultimate theoretical conversion efficiency of an ideal STPV system with no optical losses and under full solar concentration has been determined to be ~85% (Harder and Würfel, 2003). The derivation of the maximum efficiency limit is based on several restrictive constraints that cannot be achieved in real STPV systems. For instance, the maximum system efficiency is achieved at an impractical solar concentration of 46,000×, with a narrow monochromatic emission (matching the bandgap of the cell) from the emitter, and using TPV cells with no optical losses and non-radiative recombination. The narrow-band monochromatic emission requires extremely large (approaching infinity) emitter area to re-radiate the absorbed solar radiation, resulting in an impractical STPV system with nearly zero output power density (Datas and Algora, 2013a). A realistic STPV system is required to be more compact and produce adequately high output electrical power density from practically achievable input solar concentration. Therefore, the idea of monochromatic emitter needs to be abandoned and the thermal emission from the emitter is required to have a sufficient bandwidth to maximize the open circuit voltage and impedance matching in PV cells (Rephaeli and Fan, 2009). In fact, for a given bandgap of TPV cell there is an optimal non-zero emission bandwidth for which the TPV conversion efficiency is maximum (Rephaeli and Fan, 2009).

Previous thermodynamic simulation studies reported overall conversion efficiencies around 45% for less idealized STPV systems (Bermel et al., 2010; Nam et al., 2014; Rephaeli and Fan, 2009). But, to date no experimental demonstration of a STPV system has been put forth with efficiency beyond that of a standard single-junction TPV cell. Most of the early designs were based on cylindrical configurations utilizing a

centered radiator surrounded by a large cavity made of TPV cells (Datas and Algora, 2013b; Vlasov et al., 2007; Yugami et al., 2000). Owing to low radiative view factor (VF) between the emitter and TPV cells, lack of robust cooling units to prevent overheating of the TPV cells, high optical concentration losses, inefficient thermal extraction, and low area-ratio of emitter to TPV cells, their reported efficiency was poor (< 1%). In 2014, a more robust and efficient STPV system using a vertically aligned multi-walled carbon nanotube blackbody absorber and a 1-D Si/SiO2 photonic crystal as a selective emitter was built by Lenert et al. (2014). This system was a compact planar design that could be operated at much lower optical concentration, thereby enabling significant reduction in the optical losses compared to the previous designs (Datas and Algora, 2013b; Yugami et al., 2000). A narrow-bandgap InGaAsSb TPV cell (0.55 eV) was used that allowed efficient operation at lower system temperature (1285 K). The system was tested under simulated solar conditions and the efficiency of 3.2% was reported. Low conversion efficiency of the InGaAsSb TPV cell was one of the key limiting factors in their STPV design.

Ungaro et al. (2015) demonstrated a high efficiency STPV system utilizing nanostructures-based selective absorber/emitter fabricated on a W substrate and GaSb cells. The reported efficiency was 6.2% at ~1700 K. Another high-efficiency planar STPV configuration using GaSb cells was presented by Kohiyama et al. (2016) with a measured system efficiency of 5.1%. They utilized multilayer coatings of Molybdenum (Mo) and Hafnium oxide (HfO_2) on a Mo substrate for constructing a selective absorber/emitter structure. The highest STPV system efficiency reported so far was achieved by pairing a tandem plasma-interference optical filter with a 1-D Si/SiO2 photonic crystal based selective emitter (Bierman et al., 2016). The filter was engineered to reflect 80% of the sub-bandgap photons back to the emitter while allowing the in-band photons to pass through. Using an InGaAsSb cell, the reported system efficiency was 6.8%. Table 1 summarizes the key features of the selected STPV works published before (Bierman et al., 2016; Kohiyama et al., 2016; Lenert et al., 2014a; Ungaro et al., 2015). A more detailed review of previous experimental and simulated STPV systems was discussed by Gupta et al. (2018). Recently, Ni et al. (2019) presented a theoretical analysis of a low-concentration STPV system utilizing a spectrally selective five-layer metafilm (SiO2, Si3N4, W, SiO2, and W from top to bottom) absorber/emitter structure paired to an InGaAsSb TPV cell. The study also discussed the optimization of the metafilm structure to achieve > 10% system efficiency under 50 suns.

Here, we fabricated a complete planar STPV setup using a spectrally selective emitter/absorber and high-efficiency GaSb TPV cells. The spectral properties of emitter were optimized to maximize the output power density from the TPV cells. The system was tested at different operating temperatures using a high-power laser source as a simulated source of concentrated incident radiation and the experimental results are presented. Section 2 describes the experimental setup of our STPV system. A complete thermodynamic model to simulate the flow of power within the experimental setup is formulated in Section 3. The experimental results are presented in Section 4. Finally, the conclusions of this study are discussed in Section 5.

2. Experimental setup

A complete STPV system was designed comprising a planar absorber/emitter structure and GaSb TPV cells. Tungsten (W) was chosen for the absorber/emitter substrate because it preserves its structural integrity at high temperatures and possesses good intrinsic optical properties suitable for STPV applications (Datas and Algora, 2013a). The absorber and emitter were fabricated on the top and bottom surfaces of a polished W substrate (Fig. 2a) purchased from MTI Corporation. The substrate was 25.4 × 25.4 × 0.5 mm in dimensions. A 0.64 cm^2 area on its top surface was micro-textured to enhance the solar absorption. For texturing, an IPG Photonics YLP-1/30 ns 1064 nm pulsed laser operating with an average power of 24 W and 30 KHz frequency was scanned over the absorber surface by means of Galvo. The bottom surface of the W substrate served as emitter and was composed of a multilayer nanostructure to achieve spectral selectivity. The multilayer structure consists of two layers of 160 nm Si_3N_4 dielectric and a 40 nm W layer sandwiched in between as shown in Fig. 2b. The film thicknesses were computed from transfer matrix method (TMM) simulation conducted to maximize the thermal emission near the λ_{BG} (1.72 μm) of GaSb. Prior to the deposition of films, the W surface was cleaned via microwave oxygen plasma cleaning. The deposition rate of the films was calibrated based on ellipsometry measurements. Silicon nitride layers were deposited by plasma-enhanced chemical vapor deposition (PECVD) method in an Oxford Plasmalab System 100 reactor using silane and ammonia gas mixture diluted in argon. The process of mixing high and low frequency powers was employed to minimize silicon nitride film stress and, at the same time, to obtain a higher film density. The substrate temperature during deposition was maintained at 300 °C. The tungsten film was sputtered onto the substrate at room temperature from a high-purity (99.95%) W target at 90 W DC power and 0.67 Pa Ar gas pressure. The absorptance (1-R) of the micro-textured absorbing surface was measured using multiple laser sources (405 nm, 532 nm, 634 nm, 980 nm, 1064 nm, and 1342 nm) and a Labsphere RTC-060-SF integrating sphere (IS). The absorptance was found to be nearly uniform (~92%) across the wavelength of 400–1000 nm, and it drops to 87% at 1342 nm. These measurements are shown in Fig. 2c with magenta triangles along with a second order polynomial fit (magenta curve) that is later used to simulate the reflection loss for solar radiation between 0.4 μm to 2 μm. On the other hand, the specular reflectance of the emitter surface was measured using a Varian Cary 5E Spectrophotometer that has a spectral range of 300–3300 nm. The diffuse reflectance for the same surface was also measured at wavelengths 634 nm and 1342 nm using the same IS setup as used for the micro-textured absorber, and was found to be negligible (< 0.7% of the total reflection) compared to the specular reflectance. Therefore, for the thermodynamic simulation studies discussed in the next section, only the specular reflectance spectra are considered. Fig. 2c shows the simulated (red) and measured absorptivity (blue) of the fabricated emitter. Compared to plain W, the multilayer emitter surface exhibits a good spectral selectivity with increased thermal emittance right above the bandgap of GaSb TPV cell. The observed difference between the measured and simulated absorption spectra is attributed to inadequate control of the deposited film thickness. Ellipsometry measurements of the emitter surface revealed that the three films were over deposited by ~10–12% of the aimed thickness. The simulated reflectance spectra based on the film thicknesses measured by Ellipsometry (shown in green) exhibits good resemblance with the measured spectra, except at longer wavelengths

Table 1
Key features of selected experimental STPV systems reported in (Bierman et al., 2016; Kohiyama et al., 2016; Lenert et al., 2014a; Ungaro et al., 2015).

Work	Emitter structure	STPV temperature	TPV cells	System efficiency
Lenert et al. (2014)	Si/SiO_2 stack	1285 K	InGaAsSb	3.2%
Ungaro et al. (2015)	W with Si_3N_4 thin film	1700 K	GaSb	6.2%
Kohiyama et al. (2016)	Mo/HfO_2 nanostructures	1640 K	GaSb	5.1%
Bierman et al. (2016)	Si/SiO_2 stack	1273 K	InGaAsSb	6.8%

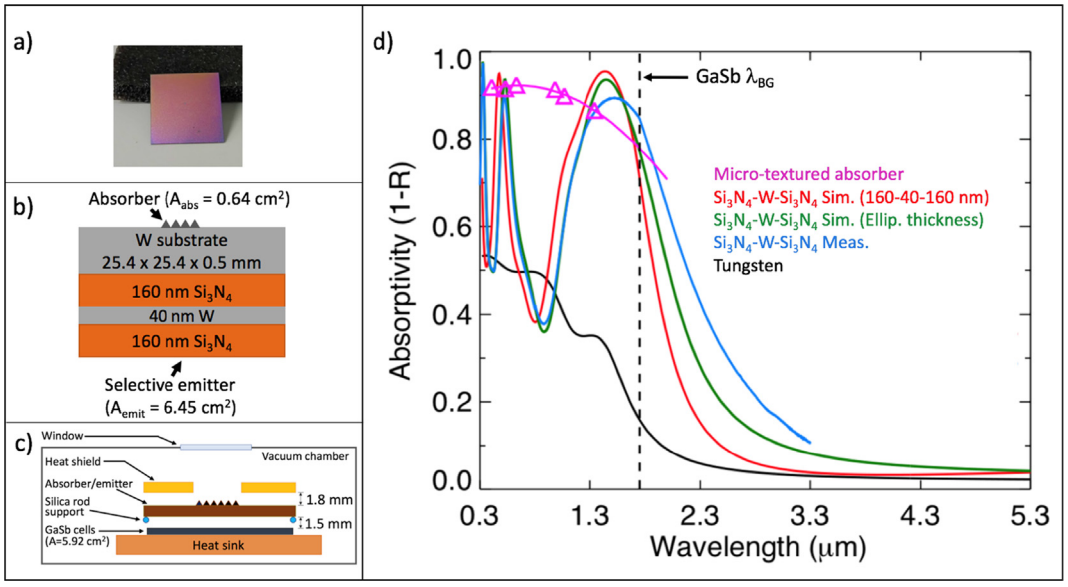

Fig. 2. (a) Picture showing the emitter side of the W substrate. (b) Schematic of the planar absorber/emitter structure. (c) Cross-sectional diagram of our experimental setup. (d) Absorptivity of micro-textured W (in magenta) and Si_3N_4-W-Si_3N_4 selective emitter (simulated results in Red and Green, and measured values in Blue). (For interpretation of the references to colour in this figure legend, the reader is referred to the web version of this article.)

where the measured absorptivity is little higher. This is most likely caused by differences in the optical constants of the materials used during fabrication and the values used in the simulation.

The GaSb TPV cells used in this experiment were purchased from JX Crystals. Four square cells, with an area of 1.48 cm^2 each (total cell area is 5.92 cm^2), were mounted on a copper substrate via reflow soldering. The cell mount was actively cooled using circulating water at 10 °C. The cells have an anti-reflection coating on top to minimize the reflection near 1.5 μm. Based on the specification provided by JX Crystals, the external quantum efficiency (EQE) of the cell peaks near 1.5 μm (JX Crystals, 2019). The reflectance spectra (Fig. 3a) of the TPV cell was measured using the spectrophotometer and is found to be ~5% (after accounting for the reflectance from the silver grid bars on the cells) near 1.4 μm, and up to 45% at sub-band wavelengths. The fill factor (FF) of the cells was measured using a quartz tungsten halogen (QTH) lamp source and found to be 0.66, which is lower than the manufacturer-reported value of 0.73 in the specification datasheet. The maximum conversion efficiency of the cells was determined experimentally for a spectrally matched narrowband input spectrum that was derived from the QTH lamp source using a 200 nm bandwidth optical bandpass filter (center wavelength at 1337 nm) purchased from PIXELTEQ. The transmittance of the band pass filter is also shown in Fig. 3a. The TPV cell efficiency was measured at a varying illumination intensity, which was controlled by the input electrical power to the QTH lamp. The output from the QTH lamp was calibrated using Thorlabs's PM100D power meter. The efficiency was measured for both the unfiltered (broadband) and matched (using the 1337-nm bandpass filter) IR radiation. The measured cell efficiency for different input illumination levels are shown in Fig. 3b. The conversion efficiency is significantly better for matched input radiation (shown by red squares) compared to that for broadband incident radiation (shown by blue triangles). This is because there is minimal thermalization and no sub-bandgap loss for the spectrally matched illumination. The maximum conversion efficiency was found to be 26.3%, which is slightly lower than the manufacturer-reported value of ~30% for spectrally matched incident radiation.

Two thin fused silica rods were used to support the W substrate over the TPV cells with a spacing of ~1.5 mm. The temperature of the substrate was measured using a type R thermocouple that was bonded to the substrate on the absorber side using the OB-600 high temperature chemical set cement purchased from OMEGA. A reflective heat shield was constructed using a gold foil mounted on an aluminum frame using the OB-600 cement. The shield was installed on the absorber side covering only the non-textured area of the W substrate. The spacing between the shield and the substrate was ~2 mm. The whole STPV assembly was installed inside a vacuum chamber to minimize convective losses. A 9.5 CFM capacity 2-stage vacuum pump was run to achieve vacuum conditions of 80 mTorr. A 300 W continuous wave

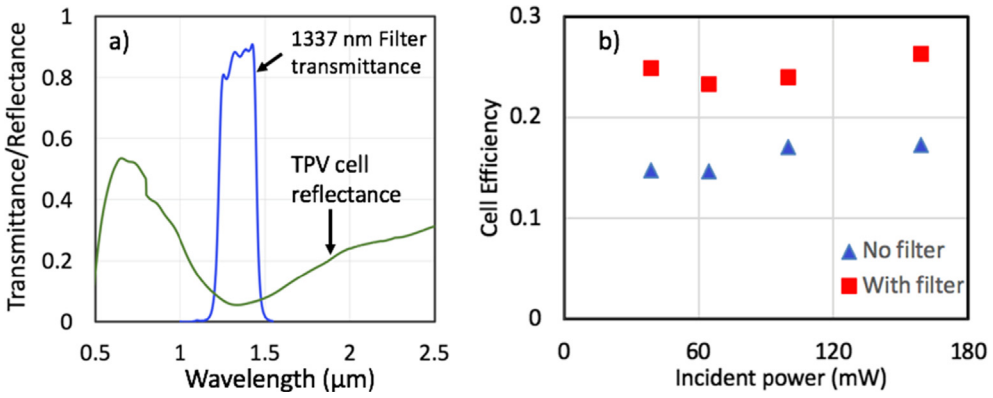

Fig. 3. (a) Plot showing the measured reflectance (in green) of the GaSb TPV cell and the transmittance curve (blue) of the 1337-nm band pass filter used to derive a narrowband thermal spectrum from a QTH lamp for characterizing the TPV cell. (b) Comparison of the measured TPV cell efficiency with a broadband IR source (blue triangles) and a selective narrowband IR emission centered at 1337 nm (red squares). (For interpretation of the references to colour in this figure legend, the reader is referred to the web version of this article.)

Table 2
Spectral selectivity, in-band emissivity, and radiant flux density computed for different emitting surfaces at T = 1676 K.

Emitter Type	η_{sel} (%)	$\varepsilon_{in\text{-}band}$	$P_{rad,emit}$ (W/cm^2)
Tungsten	69.2	0.33	5.19
Blackbody	24.7	1.00	44.73
Si_3N_4-W-Si_3N_4 Simulated	66.1	0.84	13.98
Si_3N_4-W-Si_3N_4 Measured	52.6	0.81	18.89

laser (λ = 808 nm) was setup to simulate the concentrated solar radiation in the lab. The laser was focused on the 0.64 cm^2 micro-textured absorbing surface. During the experiment, the peak power output from the GaSb cells were recorded at different operating temperatures. The maximum substrate temperature was recorded to be 1676 K for the incident laser power of 131 W.

3. STPV system modeling

A complete thermodynamic model was formulated to analyze the flow of power at multiple transport steps of the STPV system. For a given incident concentrated power (P_{in}), the emitter temperature at thermal equilibrium can be computed by solving the following equation.

$$P_{in} - P_{ref} - P_{rad,abs}(T) - P_{rad,side}(T) - P_{conv}(T) - P_{cond}(T) - P_{rad,emit}(T) = 0 \quad (1)$$

where P_{ref} is the amount of power reflected off the absorbing surface, $P_{rad,abs}(T)$ is the thermally radiated power from the absorbing surface, $P_{rad,\ side}(T)$ is the power loss due to radiation from the 4 sides of the W substrate, $P_{conv}(T)$ is the convective power loss, $P_{cond}(T)$ is the conduction loss due to silica rods and thermocouple, and $P_{rad,emit}(T)$ is the net radiant flux emitted from the emitter surface. Because the incident power in this setup is monochromatic, P_{abs} is approximately 92% of P_{in} (P_{ref} = ~8% of P_{in} at the laser wavelength based on the reflectance measurements of the microtextured W area). For actual solar incident radiation, P_{ref} slightly increases to 9.5% due to the increased reflectance of the micro-textured absorber at near-infrared wavelengths (Fig. 2c, magenta curve). The radiant flux emitted from the absorber surface ($P_{rad,abs}$) consists of two components: one radiated from a highly emissive microtextured area (A_{abs} = 0.64 cm^2), and second from the inactive or non-textured W area (5.81 cm^2). The thermal radiation emitted from a surface can be computed from Planck's function and the spectral emissivity of the surface. In our simulation, the emissivity of the involved surfaces is simply assumed to be (1-Reflectivity). The reflectance spectra of W were simulated using the optical constants provided by Rakić et al. (1998). The spectral reflectance of the W substrate was also measured between 300 and 3300 nm using the Varian Cary 5E Spectrophotometer and was found to have a good agreement with the simulated spectra. The reflectance of the microtextured area was measured. $P_{rad,\ side}$ is computed in the similar way using the emissivity of W. $P_{conv}(T)$ is simulated using equations for natural convection above a horizontal surface provided in literature (Rotem and Claassen, 1969). An adjustment factor to account for the effect of reduced pressure on natural convection was extrapolated from the work of Saidi and Abardeh (2010). The conduction loss (P_{cond}) from support was computed using fin approximation equations as described by Lenert et al. (2014a). Finally, the radiant flux power $P_{rad,emit}$ from the emitter surface was estimated using Planck's blackbody equation and the measured spectral emissivity of the surface.

One commonly used figure of merit to assess the performance of an STPV absorber/emitter is the thermal extraction efficiency (η_e), which is given by Eq. (2). To achieve high STPV system efficiency, η_e, which defines the fraction of the incident power that is delivered by the emitter to TPV cells, must be maximized. η_e is governed by both spectral and geometric properties of the absorber and emitter (Kohiyama et al., 2018). Reducing the reflection and emission losses from the absorber surface, and meanwhile, maximizing the emissivity of the emitter surface can yield in a high η_e value. The absorber-side emission losses can be suppressed by keeping the absorber area small compared to that of emitter (Kohiyama et al., 2018). The geometric control of η_e is, therefore, defined by emitter-to-absorber area ratio (AR), which is 10 in our experimental setup.

$$\eta_e = \frac{P_{rad,emit}}{P_{in}} \quad (2)$$

High η_e is necessary but not sufficient to ensure a high STPV system efficiency. Because TPV cells only responds to a limited wavelength range, it is important that the thermal emission from the emitter matches the spectral response of the cells. This characteristic of emitter is known as spectral selectivity (η_{sel}) and is defined as follows.

$$\eta_{sel} = \frac{\int_0^{\lambda_{BG}} \varepsilon(\lambda) B(\lambda, T) d\lambda}{\int_0^{\infty} \varepsilon(\lambda) B(\lambda, T) d\lambda} \quad (3)$$

where ε(λ) is the emissivity of the selective emitter, B(λ, T) is Planck's blackbody function, and λ_{BG} is the bandgap wavelength of GaSb.

In addition to high spectral selectivity, the emitter also needs to have a large effective in-band emissivity ($\varepsilon_{in\text{-}band}$), defined by Eq. (4), for maximal radiant flux power density that directly affects the TPV cell output. Table 2 summarizes η_{sel}, $\varepsilon_{in\text{-}band}$, and $P_{rad,emit}$ for W, blackbody, and Si_3N_4-W-Si_3N_4 emitters. $P_{rad,emit}$ is based on the full spectral coverage of the absorptivity, and η_{sel} provides the fraction of $P_{rad,emit}$ that is above the bandgap of the GaSb cell. Tungsten exhibits an excellent η_{sel} but poor $\varepsilon_{in\text{-}band}$. A blackbody emitter provides maximum in-band emission, but its spectral selectivity is only 24.7%. Based on the simulated reflectance spectra, the Si_3N_4-W-Si_3N_4 emitter offers high values of η_{sel} (66.1%) and $\varepsilon_{in\text{-}band}$ (0.84). η_{sel} is reduced to ~53% in the fabricated emitter sample due to the limited tolerances in the film thicknesses. The in-band radiant flux emitted by Si_3N_4-W-Si_3N_4 is nearly 3 times greater than that of W.

$$\varepsilon_{in-band} = \frac{\int_0^{\lambda_{BG}} \varepsilon(\lambda) B(\lambda, T) d\lambda}{\int_0^{\lambda_{BG}} B(\lambda, T) d\lambda} \quad (4)$$

An additional efficiency gain can be achieved by photon recycling that occurs in our STPV design on both absorber and emitter sides. The high reflectivity of the gold shield recycles the thermal radiation from the inactive absorber area back to the W substrate. The effective emittance of the inactive W area in the presence of the reflector can be modeled by Eq. (5) (Kohiyama et al., 2016; Lenert et al., 2014b), and subsequently used to simulate the suppressed emission losses. In our experimental setup, no dedicated spectral filter was installed in between the TPV cells and the emitter for recycling of the sub-bandgap emission. However, some sub-bandgap photons are reflected back to the emitter due to the non-zero reflectance of the cells at longer wavelengths (Fig. 3a). The recycling effect on the emitter side was modeled in a similar way as for the absorber side using Eq. (5). Simulation results show that the installation of the heat shield suppressed the thermal loss from the absorber side by 61%, while the cell reflectance resulted in the average sub-bandgap reflectivity of 35%.

$$\varepsilon_{Eff} = \left(\frac{1}{\varepsilon_W} + \frac{1}{1 - \varepsilon_{Au}} \right) \quad (5)$$

The overall STPV system efficiency (η_{STPV}) is modeled as:

$$\eta_{STPV} = \gamma \cdot \eta_e \cdot \eta_{sel} \cdot \eta_{PV} \quad (6)$$

where η_{PV} is the conversion efficiency of the GaSb cell and γ is the radiative VF between the emitter and TPV cells. In the simulation, the area of the TPV cells is assumed to be equal to the area of the emitting surface. The short-circuit current density (J_{sc}) is modeled by integrating

the absorbed photon flux across wavelengths less than λ_{BG}. The EQE data required for computing J_{sc} was provided by JX Crystals. The reverse saturation current density and V_{oc} of the GaSb cell as well as their dependence on cell temperature was modeled using equations and constants provided by Ferguson and Fraas (1995). Not all the radiation leaving the emitter surface reaches the cells due to a finite spacing between the two. A radiative VF between the emitter and TPV cell areas is computed to be 0.85, which implies that 15% of the energy radiated by emitter is not intercepted by the cells. This is referred as cavity loss. Because this system utilizes the standard size TPV cells and W substrates available from the manufacturers, there is a slight difference between the TPV cell and emitters areas. The emitter area is greater than the cell area by ~9%. In a custom STPV system, the two surface areas can be easily matched that would result in an improved VF of 0.91. The measured absorption spectra of the absorber and emitter surfaces were used for quantitative analysis of thermal radiation in the simulation.

When a concentrated solar radiation is incident on the absorber surface, the temperature of the absorber/emitter structure increases until thermal equilibrium is reached. The simulated steady- state absorber/emitter temperature for a given input laser power is shown in Fig. 4a. The black curve shows a case of no photon recycling. For the same input power, the STPV equilibrium temperature goes up with the installation of the gold reflector over the inactive region of the W absorber, as shown by the red curve. The combined effect of photon recycling due to the heat shield and the reflection off the GaSb cells is illustrated by the green curve. The simulation results show that the input solar concentration required to achieve the steady-state temperature of 1676 K reduces from 2718 to 1996 due to the combined photon recycling. The thermal extraction efficiency as a function of AR is plotted in Fig. 4b. The presence of the gold reflector leads to an improved η_e by reducing the thermal radiation loss from the inactive or non-textured absorber area. For AR = 10 (current experimental setup), the modeled η_e is ~78%. Fig. 4c shows the comparison between the simulated J_{sc} computed for a GaSb cell using a blackbody emitter (green) and Si_3N_4-W-Si_3N_4 selective emitter (red) as a function of the emitter temperature. J_{sc} for the selective emitter is lowered by a factor of $\varepsilon_{in\text{-}band}$ = 0.81. The simulated losses at different stages of energy transport in our STPV system operating are summarized in Table 3 for T = 1676 K. Similarly, a summary of the different simulation parameter values used to compute these losses is provided in Table 4.

Table 3
Modeled power losses at each stage of the experimental STPV system operating at T = 1676 K.

Loss item	Percent of input power
Reflection off the absorber	8%
Emission from absorber side	12.0%
Emission from sides	2.1%
Convective loss	1.7%
Conduction loss	1.0%
Cavity loss due to VF	8.4%
Sub-bandgap loss	29.8%
TPV conversion loss	19.2%
Thermalization loss	8.1%
Output electrical power	9.7%

Table 4
Summary of the different parameter values used in the simulation.

Model parameter	Value
System temperature	1676 K
Absorptivity of micro-textured W	0.92
Area of absorber/emitter substrate	6.45 cm^2
Micro-textured absorber area	0.64 cm^2
Non-textured absorber area	5.81 cm^2
Combined area of four edges of the substrate	0.51 cm^2
Thermal conductivity of the support	1.38 W/mK
Emitting surface area	6.45 cm^2
$\eta_{sel\ of\ emitter}$	52.6%
$\varepsilon_{in\text{-}band\ of\ emitter}$	0.81
$P_{rad,emit}$	18.89 W/cm^2
TPV cell area	5.92 cm^2
Distance between heat shield and absorber	1.8 mm
Distance between emitter and TPV cells	1.5 mm
VF between emitter and TPV cells	0.91
Pressure inside the chamber	80 mTorr
Temperature of TPV cells	300 K
λ_{BG} of GaSB TPV cells	1.72 μm
Reflectance of gold film (0.8–5 μm)	0.98

4. Experimental results

The STPV system was tested at various levels of incident laser power, and the corresponding absorber/emitter temperature and TPV cell output were recorded. The modeled and measured TPV cell output power density, as well as the system efficiency at different STPV temperatures are shown in Fig. 5. With increasing temperature, the thermal emission from the emitter not only increases but also exhibits better spectral matching with the EQE of the TPV cell, thereby resulting in an exponential increment in the TPV cell output and improved system efficiency. Both the measured TPV cell output and system efficiency follows the simulation curves closely. The maximum cell output power density of 1.71 W/cm^2 was recorded at a temperature of 1676 K. The corresponding incident laser power was 131 W. This value is close to the simulated P_{in} value of 126 W, thereby confirming the robustness of the simulation models. The 131 W laser beam was focused on the 0.64 cm^2 absorber area is equivalent to a solar concentration factor of ~2050 (assuming air mass of 1.5), which is within the practical limit and is achievable with Fresnel lens setup. The modeled system efficiency at 1676 K temperature is 9.7%. The experimentally measured

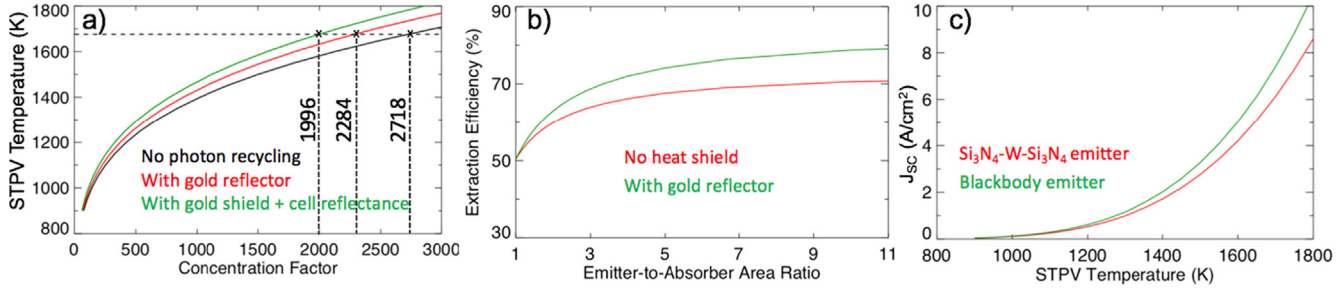

Fig. 4. (a) Simulated steady-state absorber/emitter temperature as a function of incident solar concentration. Black curve represents a case of no photon recycling. Effect of the gold reflector over the inactive area of the absorber is shown in red. Green curve shows the combined effect of photon recycling on both absorber and emitter sides. (b) Simulated extraction efficiency as a function of AR with (green) and without (red) the gold reflector. (c) Simulated J_{sc} as a function of STPV temperature for a blackbody (green) and our selective emitter (red). (For interpretation of the references to colour in this figure legend, the reader is referred to the web version of this article.)

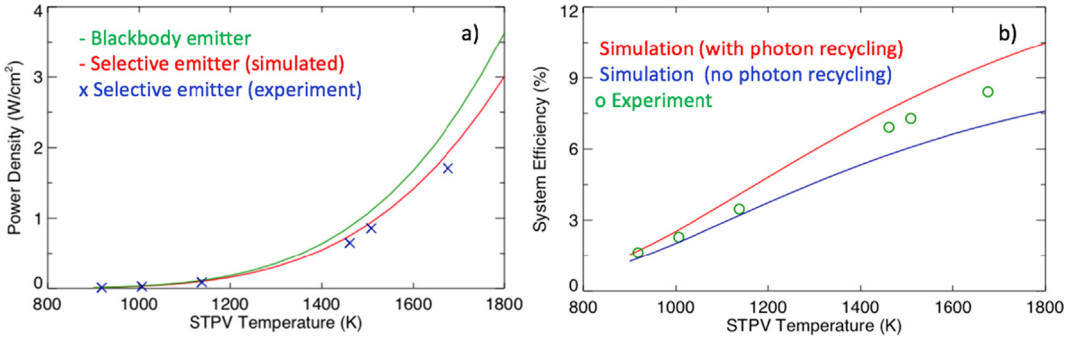

Fig. 5. (a) Experimental (Blue points) and simulated (Green curve for blackbody emitter and Red curve for our selective emitter) TPV cell output power at various absorber/emitter temperatures. (b) Modeled (Blue curve is for no photon recycling and Red curve is with photon recycling) and experimental (Green points) STPV system efficiency obtained at various operating temperatures. (For interpretation of the references to colour in this figure legend, the reader is referred to the web version of this article.)

system efficiency is 8.4%, when the TPV cell output power density is normalized to the emitting surface area. The difference between the modeled and measured system efficiency is attributable to simplified approximations incorporated at various stages of simulation. One such example is utilizing the measured absorptivity of the emitter at room temperature for simulating thermal emission at higher temperatures. In real, the optical properties of W and Si_3N_4 are temperature dependent (Barnes, 1966; Ravindra et al., 1998). Barnes (1966) reported a significant increment in the refractive index (n) of W beyond 1.5 μm at 1500 K. A TMM simulation showed that the increased 'n' value of W would result in an increased absorptivity at longer wavelengths, thereby suggesting that the actual sub-bandgap loss in our system can be larger than the modeled value listed in Table 3.

The TPV cell temperature rose to 316 K that resulted in a 5% drop in V_{oc}. For the matched portion ($\lambda < \lambda_{BG}$) of the spectral emission from the emitter, η_{PV} = 18% was achieved at 1676 K. This is lower than η_{PV} = 26% measured with a narrowband emission from the QTH lamp and filter setup. This significant reduction in the experimental η_{PV} is due to increased thermalization loss at shorter wavelengths. The thermalization loss can be suppressed by narrowing the bandwidth of the thermal emission, which will also result in a reduced output power density. Based on simulation, the optimal bandwidth for maximal system efficiency of our STPV setup is 0.4 μm right above the edge of the bandgap. The high sub-bandgap emission causes the greatest system efficiency loss (~30%) in our design. η_{sel} must be improved for suppressing the sub-bandgap loss. If the simulated spectral emission of the Si_3N_4-W-Si_3N_4 structure had been achieved for the fabricated sample, the sub-bandgap loss would have reduced by ~50% and the system efficiency would rise to 11%. Additionally, a selective window filter can also be installed in between the emitter and TPV cell for more effective recycling of sub-bandgap photons. This filter needs to be transmitive to in-band radiation, and highly reflective at wavelengths > λ_{BG}. Previous studies have reported resonance and plasma-interference filter structures based on semiconductors and transparent conducting oxides as potential edge filters for photon recycling in STPV systems (Qian et al., 2002; Vigil et al., 2005; Zenker and Heinzel, 2001). Alternatively, re-utilization of sub-bandgap photons can also be achieved using metal reflectors at the back interface of TPV cells. Recently, Omair et al. (2019) reported 94% sub-bandgap reflectivity achieved by utilizing the photovoltaic band-edge as spectral filter and incorporating a rear gold reflector in a lattice-matched $In_{0.53}Ga_{0.47}As$ TPV cell. A 75% reduction in the sub-bandgap loss in the current system would provide an additional gain of 2.4% in the system efficiency. An alternative approach of harvesting the sub-bandgap photons is by utilizing a multi-junction TPV cell structure. For example, Bendelala et al. (2018) proposed a high-efficiency TPV system comprising of a meta-material film based selective emitter coupled to an InAs/GaInAsSb tandem cell, with a theoretical maximum thermal-to-electrical conversion efficiency of ~41% at 1773 K based on simulation.

Second major loss factor is PV conversion loss (19%) in GaSb cells, which resulted mostly due to poor practical values of FF and EQE compared to much higher theoretical values reported by the manufacturer team in the specification sheet. The difference between the theoretical and practical values of FF and EQE resulted in a 3% reduction of η_{STPV}. The reflection loss from the absorber surface was found to be 8%. Reducing it to 1% would further add 0.6% gain in the system efficiency. Therefore, future works should be focused on suppressing the sub-bandgap radiation, using better TPV cells, improving the radiative VF between the emitter and cells, and reducing the reflection loss. The combination of these improvements would lead to an enhanced system efficiency of 14.5% for our planar STPV system.

The monochromatic laser radiation source used to heat up the STPV element in our experiment does not precisely simulate the broadband solar radiation. The reflectance of the micro-textured absorber is greater than 8% for longer wavelengths. The reflection loss computed for the terrestrial solar irradiance (air mass of 1.5) for wavelengths between 0.4 and 2.0 μm, which covers 95% of the incoming solar radiation, is 9.5%. Owing to this increased reflection loss from the absorbing surface, the overall system efficiency would reduce to 8.2% if tested with a realistic solar simulator, such as a conventional xenon arc light source. In addition, the optical losses in the concentrator setup should be considered when the system operates in real environment. Another essential factor in STPV system designing is the long-term thermal stability of the absorber/emitter structure. Both W and Si_3N_4 were selected for this study due to their high melting point and similar thermal expansivity (~4.5×10^{-6} K^{-1} at room temperature) (Hidnert and Sweeney, 1925; Slack and Huseby, 1982). The near-vacuum conditions during the STPV operation prevents the rapid oxidation of the W surfaces at high temperature. During the acquisition of the experimental data presented in Fig. 5, the system was operated for 5–10 min at each of the equilibrium temperatures, and no noticeable change in the TPV cell output was recorded during that short record of operation. An assessment plan is currently being formulated to study the long-term thermal stability of the proposed selective emitter and the results will be presented in a future article.

5. Conclusion

In summary, we designed and tested a high-efficiency planar STPV system using a micro-textured absorber and a multilayer metal-dielectric (Si_3N_4-W-Si_3N_4) coating-based selective emitter. High thermal extraction and effective recycling of the sub-bandgap photons are key to achieve high system efficiency. The in-band thermal emission for our selective emitter was measured nearly 3 times greater than that of a W emitter. The excellent thermal management, where the TPV cells were mounted on a water-cooled copper heat sink, prevented excessive

heating of the cells during operation. The near-equal planar areas of the emitting surface and TPV cells with a separation distance of only 1.5 mm between the two resulted in a high radiative VF of 0.85, thereby significantly reducing the cavity loss. The implementation of a gold-based heat shield also suppressed the undesired thermal emission from the absorber side by ~61%. We measured a high output power density of 1.71 W/cm^2 and a system efficiency of 8.4% at the operating system temperature of 1676 K using a 300 W continuous wave laser for incident radiation. For a broadband solar concentration input, the system efficiency would reduce to 8.2% due to the increased reflection loss from the absorbing surface, especially at near-infrared wavelengths. The required incident solar concentration to achieve this efficiency is 2100X at air mass of 1.5. Our experimental efficiency is higher than those of previously reported STPV systems and this can be improved further by incorporating a better recycling scheme to reflect unconvertable photons back to the emitter and by using more efficient GaSb cells.

Declaration of Competing Interest

The authors declare that they have no known competing financial interests or personal relationships that could have appeared to influence the work reported in this paper.

Acknowledgments

We thank the NASA Langley Professor program and NSF IUCRC Center for the financial support. A portion of this research was conducted at the Center for Nanophase Materials Sciences, which is sponsored at Oak Ridge National Laboratory by the Scientific User Facilities Division, Office of Basic Energy Sciences, U.S. Department of Energy.

References

Barnes, B.T., 1966. Optical Constants of Incandescent Refractory Metals. J. Opt. Soc. Am. 56, 1546. https://doi.org/10.1364/josa.56.001546.

Bendelala, F., Cheknane, A., Hilal, H., 2018. Enhanced low-gap thermophotovoltaic cell efficiency for a wide temperature range based on a selective meta-material emitter. Sol. Energy 174, 1053–1057. https://doi.org/10.1016/j.solener.2018.10.006.

Bermel, P., Ghebrebrhan, M., Chan, W., Yeng, Y.X., Araghchini, M., Hamam, R., Marton, C.H., Jensen, K.F., Soljačić, M., Joannopoulos, J.D., Johnson, S.G., Celanovic, I., 2010. Design and global optimization of high-efficiency thermophotovoltaic systems. Opt. Express 18, A314. https://doi.org/10.1364/oe.18.00a314.

Bierman, D.M., Lenert, A., Chan, W.R., Bhatia, B., Celanović, I., Soljačić, M., Wang, E.N., 2016. Enhanced photovoltaic energy conversion using thermally based spectral shaping. Nat. Energy 1, 16068. https://doi.org/10.1038/nenergy.2016.68.

Crystals, J., n.d. Specification sheet for GaSb cells [WWW Document].

Datas, A., 2015. Optimum semiconductor bandgaps in single junction and multijunction thermophotovoltaic converters. Sol. Energy Mater. Sol. Cells 134, 275–290. https://doi.org/10.1016/j.solmat.2014.11.049.

Datas, A., Algora, C., 2013a. Global optimization of solar thermophotovoltaic systems. Prog. Photovoltaics Res. Appl. 21, 1040–1055. https://doi.org/10.1002/pip.2202.

Datas, Alejandro, Algora, C., 2013b. Development and experimental evaluation of a complete solar thermophotovoltaic system. Prog. Photovoltaics Res. Appl. 21, 1025–1039. https://doi.org/10.1002/pip.2201.

Ferguson, L.G., Fraas, L.M., 1995. Theoretical study of GaSb PV cells efficiency as a function of temperature. Sol. Energy Mater. Sol. Cells 39, 11–18.

Gupta, M.C., Ungaro, C., Foley, J.J., Gray, S.K., 2018. Optical nanostructures design, fabrication, and applications for solar/thermal energy conversion. Sol. Energy 165, 100–114. https://doi.org/10.1016/j.solener.2018.01.010.

Harder, N.P., Würfel, P., 2003. Theoretical limits of thermophotovoltaic solar energy conversion. Semicond. Sci. Technol. 18. https://doi.org/10.1088/0268-1242/18/5/303.

Hidnert, P., Sweeney, W.T., 1925. Thermal expansion of tungsten. Sci. Pap. BS 20, S515.

Kohiyama, A., Shimizu, M., Yugami, H., 2018. Radiative heat transfer enhancement using geometric and spectral control for achieving high-efficiency solar-thermo-photovoltaic systems. Jpn. J. Appl. Phys. 57. https://doi.org/10.7567/JJAP.57.040312.

Kohiyama, A., Shimizu, M., Yugami, H., 2016. Unidirectional radiative heat transfer with a spectrally selective planar absorber/emitter for high-efficiency solar thermo-photovoltaic systems. Appl. Phys. Express 9, 112302. https://doi.org/10.7567/APEX.9.112302.

Lenert, A., Bierman, D.M., Nam, Y., Chan, W.R., Celanović, I., Soljačić, M., Wang, E.N., 2014a. A nanophotonic solar thermophotovoltaic device. Nat. Nanotechnol. 9, 126–130. https://doi.org/10.1038/nnano.2013.286.

Lenert, A., Nam, Y., Bierman, D.M., Wang, E.N., 2014b. Role of spectral non-idealities in the design of solar thermophotovoltaics. Opt. Express 22, A1604. https://doi.org/10.1364/oe.22.0a1604.

Nam, Y., Yeng, Y.X., Lenert, A., Bermel, P., Celanovic, I., Soljačić, M., Wang, E.N., 2014. Solar thermophotovoltaic energy conversion systems with two-dimensional tantalum photonic crystal absorbers and emitters. Sol. Energy Mater. Sol. Cells 122, 287–296. https://doi.org/10.1016/j.solmat.2013.12.012.

Ni, Q., McBurney, R., Alshehri, H., Wang, L., 2019. Theoretical analysis of solar thermophotovoltaic energy conversion with selective metafilm and cavity reflector. Sol. Energy 191, 623–628. https://doi.org/10.1016/j.solener.2019.09.033.

Omair, Z., Scranton, G., Pazos-Outon, L., Xiao, T., Steiner, M., Ganapati, V., Peterson, P., Holzrichter, J., Atwater, H., Yablonovitch, E., 2019. Ultraefficient thermophotovoltaic power conversion by band-edge spectral filtering. Proc. of the. Natl. Acad. Sci. 116 (31), 15356–15361. https://doi.org/10.1073/pnas.1903001116.

Qian, Z.G., Shen, W.Z., Ogawa, H., Guo, Q.X., 2002. Infrared reflection characteristics in InN thin films grown by magnetron sputtering for the application of plasma filters. J. Appl. Phys. 92, 3683–3687. https://doi.org/10.1063/1.1506199.

Rakić, A.D., Djurišić, A.B., Elazar, J.M., Majewski, M.L., 1998. Optical properties of metallic films for vertical-cavity optoelectronic devices. Appl. Opt. 37, 5271. https://doi.org/10.1364/ao.37.005271.

Ravindra, N.M., Abedrabbo, S., Chen, W., Tong, F.M., Nanda, A.K., Speranza, A.C., 1998. Temperature-dependent emissivity of silicon-related materials and structures. IEEE Trans. Semicond. Manuf. 11, 30–39. https://doi.org/10.1109/66.661282.

Rephaeli, E., Fan, S., 2009. Absorber and emitter for solar thermo-photovoltaic systems to achieve efficiency exceeding the Shockley-Queisser limit. Opt. Express 17, 15145. https://doi.org/10.1364/oe.17.015145.

Rotem, Z., Claassen, L., 1969. Natural convection above unconfined horizontal surfaces. J. Fluid Mech. 39, 173–192. https://doi.org/10.1017/S0022112069002102.

Rühle, S., 2016. Tabulated values of the Shockley-Queisser limit for single junction solar cells. Sol. Energy 130, 139–147. https://doi.org/10.1016/j.solener.2016.02.015.

Saidi, M., Abardeh, R.H., 2010. Air pressure dependence of natural-convection heat transfer. In: WCE 2010 - World Congress on Engineering 2010. pp. 1444–1447.

Shockley, W., Queisser, H.J., 1961. Detailed balance limit of efficiency of p-n junction solar cells. J. Appl. Phys. 32, 510–519. https://doi.org/10.1063/1.1736034.

Slack, G.A., Huseby, I.C., 1982. Thermal Grüneisen parameters of CdAl2O4, β–Si3N4, and other phenacite-type compounds. J. Appl. Phys. 53, 6817.

Ungaro, C., Gray, S.K., Gupta, M.C., 2015. Solar thermophotovoltaic system using nanostructures. Opt. Express 23, A1149. https://doi.org/10.1364/oe.23.0a1149.

Vigil, O., Ruiz, C.M., Seuret, D., Bermúdez, V., Diéguez, E., 2005. Transparent conducting oxides as selective filters in thermophotovoltaic devices. J. Phys. Condens. Matter. https://doi.org/10.1088/0953-8984/17/41/008.

Vlasov, A.S., Khvostikov, V.P., Khvostikova, O.A., Gazaryan, P.Y., Sorokina, S.V., Andreev, V.M., 2007. TPV systems with solar powered tungsten emitters. AIP Conf. Proc. 327–334. https://doi.org/10.1063/1.2711750.

Yugami, H., Sai, H., Nakamura, K., Nakagawa, N., Ohtsubo, H., 2000. Solar thermo-photovoltaic using Al2O3/Er3Al5O12eutectic composite selective emitter. In: Conference Record of the IEEE Photovoltaic Specialists Conference, pp. 1214–1217.

Zenker, M., Heinzel, A., 2001. Efficiency and power density potential of combustion-driven thermophotovoltaic systems using GaSb photovoltaic cells. IEEE Trans. Electron Devices 48, 367–376. https://doi.org/10.1109/16.902740.